Aging of the microstructure of melt-textured $YBa_2Cu_3O_7/Y_2BaCuO_5$ composites and implications on their superconducting properties

F. Sandiumenge, N. Vilalta, S. Piñol, B. Martínez, and X. Obradors
Institut de Ciència de Materials de Barcelona, Consell Superior d'Investigacions Científiques, Campus de la Universitat Autònoma de Barcelona, 08193 Bellaterra, Catalunya, Spain
(Received 3 October 1994)

The aging process of the microstructure and superconducting properties of $YBa_2Cu_3O_7/Y_2BaCuO_5$ directionally solidified composites has been observed upon increasing the oxygenation time. The process is characterized by an increase of the dislocation density up to a maximum of 1.3×10^{10} cm^{-2} and the formation of large stacking faults, preferentially from low-angle grain boundaries and around Y_2BaCuO_5 precipitates, as well as an intense degradation of the $YBa_2Cu_3O_7$ matrix at either side of the microcracks and around the precipitates. The stacking faults propagate more easily along the ⟨100⟩ directions and the shear component of their associated displacement vectors is exchanged between the *a* and *b* axis directions at every twin boundary. Both stacking faults and matrix degradation occur along the (001) planes, giving rise to a pronounced two-dimensionality of the aged microstructure. The aging of the microstructure is accompanied by a strong field-dependent reduction of the critical currents leading to a downward shift of the irreversibility line. Low-field ac susceptibility measurements with $\mathbf{H}\|ab$ confirm an enhanced two-dimensional behavior associated with the layered defective microstructure. It is shown that the rate at which these layered defects are generated depends on the content of Y_2BaCuO_5 phase in the samples.

I. INTRODUCTION

It is well established nowadays that oxygen stoichiometry is crucial in determining the superconducting performance of $YBa_2Cu_3O_{7-x}$ oxides. It has been argued that even for the stoichiometric ($x\sim0$) compound, local fluctuations of oxygen content exist, which may affect the flux-pinning characteristics of the compound.[1] On the other hand, to obtain the optimum uniform oxygenation of bulk textured samples is not an easy task. The usual way to achieve oxygen stoichiometry in [$YBa_2Cu_3O_7$(123)]/[Y_2BaCuO_5(211)] textured composites is the annealing of the samples in an O_2 flow. This process requires heating of the samples between 400 and 500 °C. However, it appears that a proper choice of the two process variables, namely, annealing time and temperature, is difficult and has dramatic consequences in the superconducting properties of the materials. For instance, it has been shown that a layered oxygen deficiency modifies the critical currents and the irreversibility line.[2] Ozone oxygenation at lower temperatures for few hours has been proposed as an alternative,[3] but is was shown that the microstructure can be strongly degraded unless the process variables are well adjusted. A strong dependence of both the irreversibility line and $J_c(H)$ on the annealing time has recently been reported,[4] making evident the pernicious effect of an excessively long annealing process. The reported observation of strong modifications of the irreversible superconducting properties suggests that important modifications of the microstructure occur during the oxygenation step. Therefore an important issue still to be fully elucidated is how overexposure to an oxygen atmosphere at typical annealing temperatures affects the microstructure of 123/211 highly aligned composites. This investigation may, in turn, allow deeper insights into those defects which are relevant for flux pinning by comparing the microstructure and field dependence of the critical currents of nonaged with aged samples. A detailed characterization of the microstructure of our directionally solidified 123/211 composites has already been published.[5]

II. EXPERIMENT

The samples used in this study were grown using a vertical Bridgman technique described elsewhere.[5] Oxygenation experiments were performed on whole bars having as typical dimensions $10\times0.3\times0.3$ cm^3, from which single-domain samples were extracted. The final content of the 211 phase in the composite was determined by measuring the paramagnetic susceptibility of the sample and fitting a Curie-Weiss law in the high-temperature range ($T>120$ K). Then the actual 211 phase percentage may be obtained through the relation $(\mu_{obs}/\mu_{211})^2\times100$, μ_{obs} being the magnetic moment obtained from the Curie-Weiss law and μ_{211} the magnetic moment of the 211 pure phase.

The observations of the aged microstructure were performed using transmission electron microscopy (TEM) on samples containing between 31 and 36 vol% of 211 which were oxygenated for 156 h at 450 °C. These samples were cut with a diamond saw placed parallel and perpendicular to either the (001) or *ab* planes to allow observations along the [001] and [100] zone axes, respectively. Care was taken to avoid contact of the specimens with water. The slices were then mechanically polished down to ~30 μm and ion milled at reduced voltages (4 kV) and currents (0.3 mA) and cooled by a cold finger immersed in liquid nitrogen to avoid damage of the samples. TEM

observations were performed in the Philips CM30 electron microscope at 200 kV.

Low-field dc and ac susceptibility measurements were carried out to investigate when a full screening of the sample occurs. Inductive critical currents and the irreversibility line were deduced from magnetization measurements performed with a superconducting quantum interference device (SQUID) magnetometer. The typical size of the samples used in these magnetization measurements was $2\times1.5\times0.5$ mm^3 with the longer dimensions directed parallel to the magnetic field to minimize self-field effects. The critical currents were calculated from the generalized Bean model where $J_c^{ab}\approx 20\Delta M/L_1[1-L_1/3L_2]$ and $J_c^c\approx 20\Delta M/L_2$, where $L_1\leq L_2$ are the sides limiting the surface perpendicular to the applied field and ΔM is the difference between the upper and lower branches of the $M(H)$ loops. The magnetic measurements were performed on two different type of samples having different concentrations of 211 precipitates, each one being oxygenated during progressively longer times. First a sample having 36% of the 211 phase was slowly cooled (40 K/h) in air from 900 °C to room temperature (this sample is hereafter referred to as "as grown"). Later on, isothermal annealings in flowing O_2 at 450 °C for 60 and 156 h were carried out. Second, a sample with 14% of 211 phase was studied. This sample was quenched from 900 °C in air and subsequently annealed at 450 °C in flowing O_2 for 72, 120, and 700 h.

III. RESULTS

A. Observations along the [001] zone axis

The most apparent feature of the aged microstructure is a drastic increase of the dislocation density within the 123 matrix up to 1.3×10^{10} cm^{-2}, as compared with the maximum value of 10^9 cm^{-2} found in similar nonaged samples.[5] This resembles the densities achieved by shock-treated[6] and mechanically deformed[7] samples, and is even close to the density reported for some as-solidified samples processed using a modified Bridgman technique.[8] Dislocations may appear as long undissociated segments with intense associated strain contrast, in particular when crossing twin boundaries. Dislocations also appear as extended dissociated short segments[9] densely distributed along wide areas as imaged with $\mathbf{g}=200$ in Fig. 1(a), where both perfect and partial dislocations are visible. When dislocation lines are perpendicular to the twin boundaries, the latter behave as pinning sites and dislocation segments bow out between consecutive twin boundaries [arrowed in the upper part of Fig. 1(a)]. In other instances it is observed that the dislocations propagate unaffected across twin boundaries, or when the dislocation line is not perpendicular to the twin boundaries, short segments are locked in the twin boundary, as arrowed in the lower part of Fig. 1(a). These dislocation-twin interaction modes have been discussed previously for 123 samples deformed at room temperature[10] and indicate that the aging process induces a severe plastic deformation of the orthorhombic 123 phase. Figures 1(b) and 1(c) show the contrast behavior of one isolated dissociated segment. When imaged with $\mathbf{g}=110$, that is, with the diffraction vector perpendicular to the twin planes [Fig. 1(b)], the region enclosed between the dissociated branches displays stacking-fault contrast. The contrast appears homogeneous because the stacking fault is parallel to the surface of the foil. It can be observed that the stacking fault is divided by a dislocation. In a dark-field image with $\mathbf{g}=-110$ (not shown), the stacking fault was visible at either side of the dislocation, while the dislocation itself was out of contrast, and when imaged with $\mathbf{g}=100$ [Fig. 1(c)] it is observed that the part of the stacking fault located below the dislocation as well as its bounding partial dislocation are out of contrast.

Stacking faults in the 123 phase have been found to consist of an additional CuO chain layer adjacent to the BaO plane, giving rise to a double chain layer or local 124 structure[11] with an associated shear in-plane component of the displacement vector of $\frac{1}{2}[010]$ (preventing atoms of the same nature from being in first-neighbor positions) and an expansion of the matrix of $c/6$ (height of one single layer). Therefore, since the stacking-fault contrast must be maximum for $\alpha=2\pi\mathbf{g}\cdot\mathbf{R}=(2n+1)\pi$ and

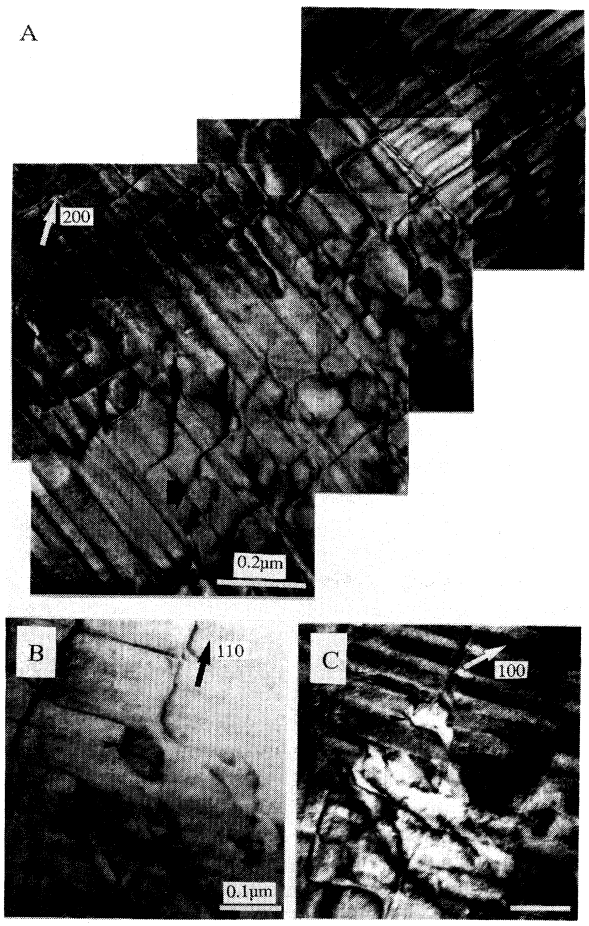

FIG. 1. (a) Bright-field image obtained with the 200 reflection near the Bragg position showing extensive dislocation dissociation; (b) bright field, $\mathbf{g}=110$; (c) bright field, $\mathbf{g}=100$.

zero for $\alpha=0$ or $2\pi n$ (here n is an integer and **R** is the displacement vector), the above observations are consistent with $\mathbf{R}=\frac{1}{6}[103]$ and $\mathbf{R}=\frac{1}{6}[013]$,[12] alternating across the central dislocation. Our contrast analysis is consistent with the dissociation scheme

$$[110]\rightarrow\tfrac{1}{6}[301]+\tfrac{1}{2}[110]+\tfrac{1}{6}[03\bar{1}]$$

proposed by Rabier, Tall, and Denanot for samples deformed at room temperature under hydrostatic pressure (see Ref. 9 for details), and this dissociation mechanism is accompanied by the nucleation of stacking faults at the dislocation cores. It is thus very appealing to suggest that, as far as the plastic deformation of the matrix is concerned, similar effects to those achieved after the mechanical deformation of the samples resulted from a prolonged annealing process in an oxygen flow at 450 °C.

Stacking faults were also found to originate from low-angle grain boundaries, 211/123 interfaces, and matrix degraded regions associated with microcracks, as discussed below. The contrast behavior of these stacking faults is shown in Figs. 2(a)–2(c) for the case where they originate from a low-angle grain boundary [the boundary is arrowed in the photographs and is clearly visible in Fig. 2(b)]. The photographs show stacking faults elongated in one of the two mutually perpendicular ⟨100⟩ directions, imaged under different two-beam conditions. A misorientation of 3° was found by comparing the selected area diffraction (SAD) patterns obtained at either side of the boundary. When imaging the side of the grain boundary not shown in Fig. 2, a similar microstructure to that analyzed below was observed. With $\mathbf{g}=110$ [Fig. 2(a)], that is, with the operative diffraction vector normal to the twin boundaries, twin contrast is avoided and both types of stacking faults, directed along [100] and [010], are visible simultaneously. For $\mathbf{g}=200$ and $\mathbf{g}=020$ [Figs. 2(b) and 2(c), respectively] both stacking faults are simultaneously out of contrast, while when the **g** vector is parallel to their bounding partial dislocations these are visible and there is no contrast change when passing from one twin variant to the other. That indicates that for the same twin variant the Burgers vector associated with the stacking fault long in the [100] direction has an in-plane shear component directed along [100], while that associated with the stacking fault long in the [010] direction is directed along [010], and both alternate across the twin boundaries. The fault contrast behavior is consistent again with $\mathbf{R}=\frac{1}{6}[103]$ and $\mathbf{R}=\frac{1}{6}[013]$. Finally, the two ⟨110⟩ dislocations which also originate from the grain boundary are visible under the diffraction conditions used in Figs. 2(a)–2(c) but were out of contrast with $\mathbf{g}=-110$ (not shown). According to the $\mathbf{g}\cdot\mathbf{b}=0$ invisibility criterion, this behavior is consistent with a pure screw character and the Burgers vector directed along [110].

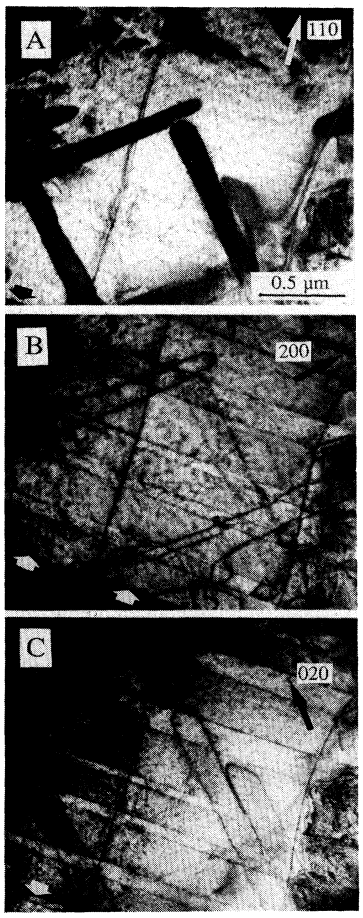

FIG. 2. Two-beam bright-field images of stacking faults originating from a low-angle grain boundary imaged with the 110 (a), 200 (b), and 020 (c) reflections at the Bragg position.

It was observed that the stacking faults associated with 211/123 interfaces are more abundant and larger than those associated with the low-angle grain boundaries as illustrated in Fig. 3(a). The fact that all the stacking faults shown in the image originate far from the thin edge of the specimen rules out the possibility that they resulted from the ion-milling process or moisture uptake. The inset of Fig. 3(a) is an enlarged view of the area enclosed by a white border showing several dislocation loops enclosing small stacking faults (arrowed), as identified by diffraction contrast. Similar loops have been reported for melt-processed 123/211 thick-film composites around 211 precipitates[13] and for single crystals grown by the flux method.[14] Stacking faults elongated in one of the two mutually perpendicular ⟨100⟩ directions extend up to more than 2 μm away from the 211/123 interface from which they were originated. The stacking faults appear wide at the origin while transforming to a fingerlike pattern away from the interface, suggesting that, being initially narrower, they merge laterally after some aging period. The central region of the photograph also shows a degraded region where the twin contrast is almost lost (arrowed) from which similar stacking faults propagate toward the thin edge of the specimen. It is worth mentioning that all the stacking faults characteristic of the aged microstructure are elongated along the [100] and [010] matrix directions, indicating that the growth rate of the inserted CuO chain layer is larger along the Cu-O chain direction.

Another observed effective stacking-fault source is

dislocation tangles, as shown in Fig. 3(b), where pipe diffusion is probably an efficient feeding mechanism for the growth of the stacking faults; however their size is typically smaller than that corresponding to the stacking faults originating from the 211/123 interfaces [compare Figs. 3(a) and 3(b)].

B. Observations along the [100] zone axis

Further understanding of the development of the defect structures associated with the 211/123 interfaces and the degraded matrix region shown in Fig. 3 may be gained by viewing the specimens along the [100] zone axis. Figure 4 shows the interaction of a microcrack with a 211 particle in a sample oxygenated for 156 h (aged) (a) and in a sample oxygenated for 60 h (nonaged) (b). The matrix region adjacent to the interaction region is highly defective, even degraded. In 123/211 composites, microcracks constitute the preferential diffusion path for oxygen during the annealing process.[2] The microcracks shown in Fig. 4 present a strongly defective layer at either side of the gap, which constitutes the signature of an intense oxidation-driven degradation of the matrix, in agreement with previous decomposition studies,[15] and it has been shown that the gap itself is filled with Cu-rich phases.[5] It was observed that the twins often disappear when approaching the degraded layers [see Fig. 4(a)] suggesting that the orthorhombic crystal structure is lost. The width of the gap including the associated degraded layers is increased noticeably from the nonaged sample [Fig. 4(b)] to the aged sample [Fig. 4(a)], in particular, when approaching the 211 precipitate, and the gap itself is widened at the intercept with the 211 precipitate in the aged sample [Fig. 4(a)]. Thin degraded layers also parallel to the *ab* planes may be observed not associated with the microcracks, as arrowed in Fig. 4(a). The most striking feature in the figures is a drastic increase in size of the defective region around the region of interaction between the microcrack and the 211 precipitate, thus signaling an enhanced oxygen diffusion region at either side of the microcrack and along the 211/123 interface. Once oxygen

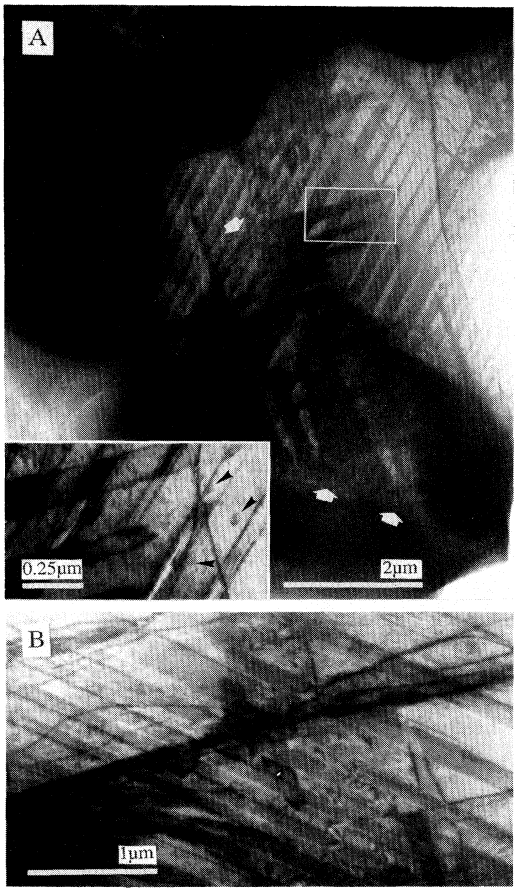

FIG. 3. (a) Large stacking faults elongated in the [100] and [010] directions originating from 211/123 interfaces and a degraded zone (arrowed). The inset is an enlarged view of the region enclosed by white borders, where small dislocation loops are indicated by arrow heads. (b) Similar stacking faults originating from a dislocation tangle.

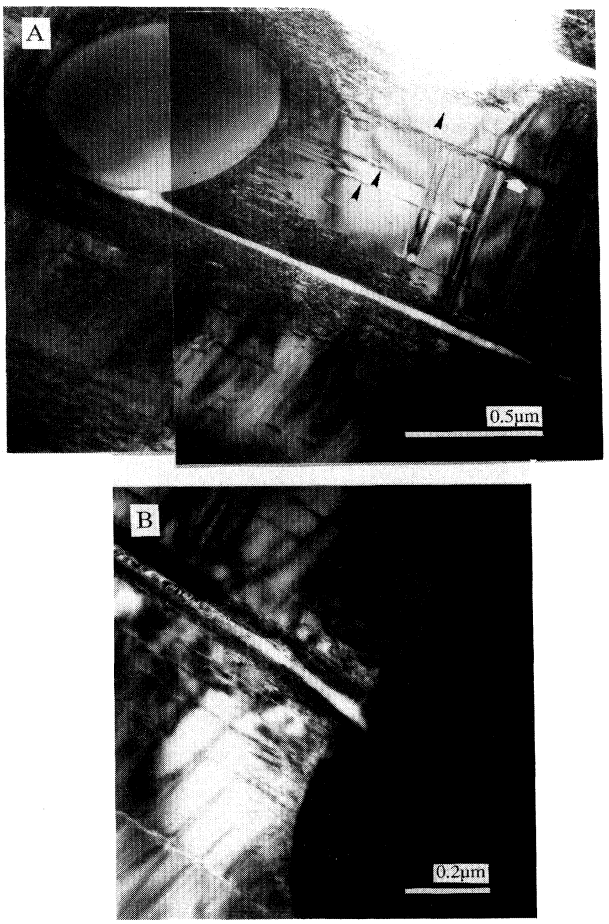

FIG. 4. Interaction of a microcrack with a 211 precipitate with associated thick degraded layers viewed along the [100] direction: (a) aged sample, oxygenated for 156 h, and (b) nonaged sample, oxygenated for 60 h.

has diffused along the 211/123 interface, then it can be assumed that at moderate temperatures and sufficiently long oxygenation periods oxygen can diffuse along the (001) planes, provided that the atomic diffusion is always easier along these planes than along the c axis.[16] However, Fig. 4(a) also shows that under these conditions the degraded region may even extend in the direction normal to the (001) planes, thus overlapping with the degraded regions associated with neighboring precipitates [the upper precipitate in Fig. 4(a) was lost during the ion-milling process]. Here, atomic mobility is also likely to be favored by the stress state of the matrix revealed by the intense strain contrast. Stacking faults, indicated by arrowheads in Fig. 4(a), are also visible associated with the 211/123 interface and the degraded regions, and degradation is frequently observed along their traces.

Finally, let us address the consequences of the aging process on the mechanical properties of the composite. TEM observations of the nonaged samples showed that, generally, the 211 precipitates are well bonded to the surrounding matrix and accordingly the microcracks are effectively stopped at their interfaces.[5] The interaction is often accompanied by complex defect structures within the precipitate, thus suggesting that the propagation energy of the microcrack is absorbed by the precipitate through severe plastic deformation.[5] In the aged samples, the above observations have revealed a strong degradation of the microstructure. These effects are likely to decrease the mechanical toughness of the aged composites. Figure 5 shows a microcrack propagating across a 211 precipitate, which never happens in the nonaged samples. This phenomenon was found in several precipitates. It is well known that the thermal contraction of the 123 matrix is higher along the c axis than perpendicular to it. As a result, the precipitates are subjected to a persistent tensile stress at the regions adjacent to their intercept with a microcrack. In addition, in the aged samples, the matrix degradation process is probably associated with a volume reduction, as indicated by the widening of the microcrack shown in Fig. 4(a). We believe that both considerations could be at the origin of the observed propagation of microcracks across the 211 precipitates.

C. Superconducting properties

The superconducting properties of samples containing 14% and 36% of 211 phase have been studied by using a SQUID magnetometer and an ac susceptometer. Field and temperature dependencies of the critical currents have been investigated with the external applied field parallel to the c axis ($\mathbf{H}\|c$) and parallel to the ab planes ($\mathbf{H}\|ab$). Low-field zero-field-cooled susceptibility measurements have been performed with both field orientations ($\mathbf{H}\|ab$ and $\mathbf{H}\|c$), showing that while in the as-grown sample complete shielding is achieved in both cases, for the sample annealed for 156 h complete shielding is only reached for $\mathbf{H}\|c$; for $\mathbf{H}\|ab$ the shielding only amounts to about 30% of the total volume (for $H_{dc}=10$ Oe) (see Fig. 6) and slightly increases at low temperatures for smaller fields (an increase of the shielding capacity of about 15% is observed in the ac susceptibility when decreasing the ac field from 10 to 0.1 Oe). These results are in good agreement with the observed increase of the c-axis component of the normal-state resistivity in aged samples[17] and give strong indications of a layered degradation of the sample leading to a quasilayered structure in which nonsuperconducting degraded areas and superconducting zones are stacked along the c axis.

In Fig. 7 typical hysteresis cycles at $T=77$ K with the $\mathbf{H}\|c$ field orientation as a function of the annealing time in O_2 for the 36% 211 sample are displayed. A strong decrease of the irreversibility region for the longest annealing period (156 h) is the first feature apparent from the figure; nevertheless, differences are very small in the low-field region. This behavior may be more clearly appreciated in Fig. 8, where we show the field dependence of the critical currents at two temperatures for both field orientations. As we have already commented, in the low-field

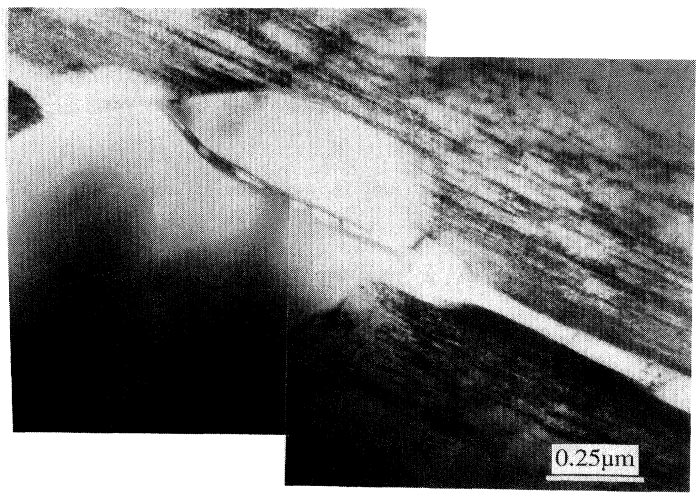

FIG. 5. Microcrack propagating across a 211 particle.

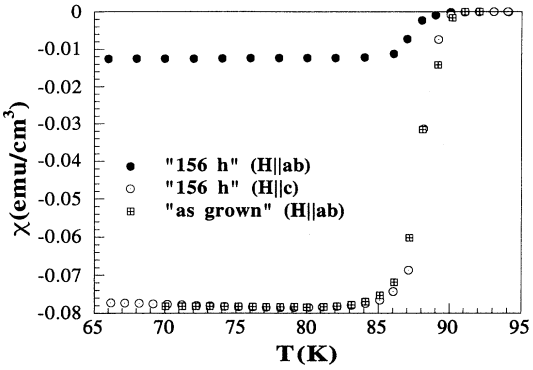

FIG. 6. Low-field dc susceptibility ($H=10$ Oe) showing the dependence of the shielding capability on the annealing time and field orientation.

region (up to few thousand gauss) differences are small but they become more important as the field increases. In that case the differences turn out to be dependent on temperature and field orientation.

This is also clearly reflected in the irreversibility line in the $\mathbf{H}\|c$ configuration (see Fig. 9) in which a dramatic downward shift for the 156-h annealed sample is observed. Similar features are observed in the $\mathbf{H}\|ab$ configuration, but, in contrast with what was observed in

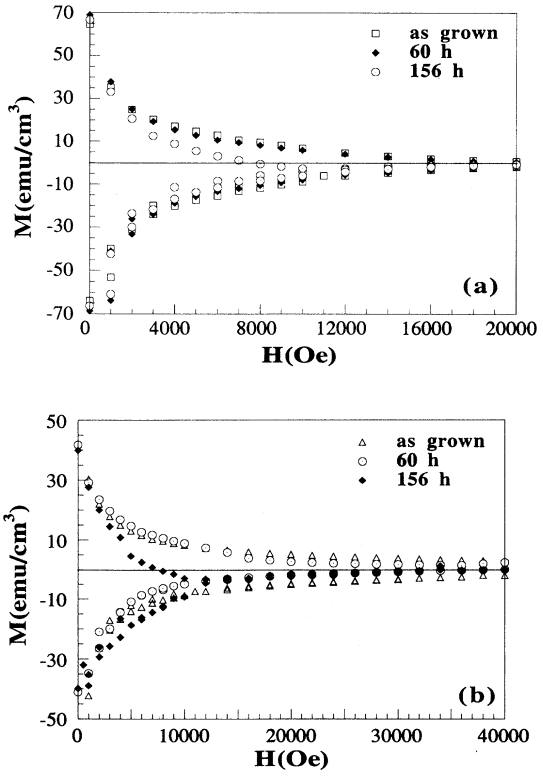

FIG. 7. Hysteresis loops of melt-textured $YBa_2Cu_3O_7$-Y_2BaCuO_5 composites at $T=77$ K as a function of the O_2 annealing time for $\mathbf{H}\|c$ (a) and $\mathbf{H}\|ab$ (b).

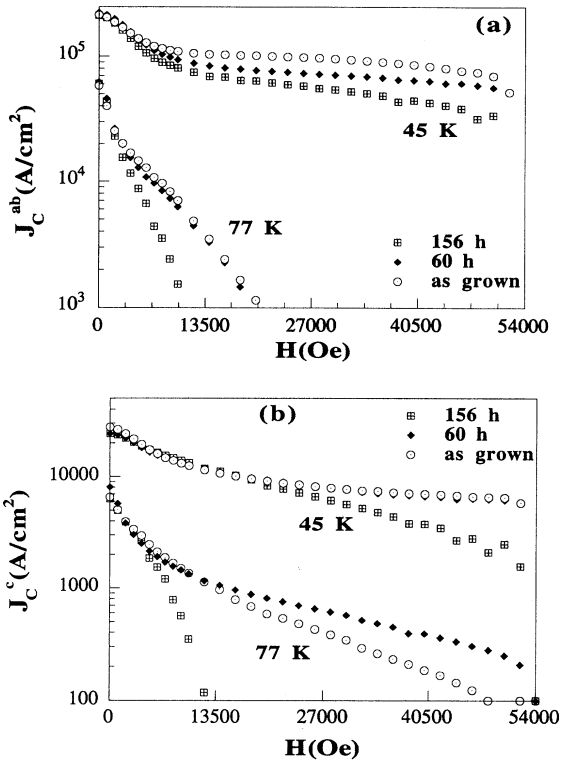

FIG. 8. Inductive critical currents at $T=45$ and 77 K as a function of the O_2 annealing time for $\mathbf{H}\|c$ (a) and $\mathbf{H}\|ab$ (b).

oxygen-deficient melt-textured $YBa_2Cu_3O_{7-x}$,[2] in this case the most impressive shift is observed in the $\mathbf{H}\|c$ configuration.

In addition, the oxygen annealing process has also been studied in a sample with low 211 phase concentration ($\approx 14\%$) in which an anomalous $J_c^{ab}(H)$ dependence (fishtail effect) is observed. As in the case of the samples containing 36% of 211 phase, a deterioration of the superconducting properties, increasing the annealing time, is evident from the behavior of the inductive critical currents (see Fig. 10). Overall, however, the degradation

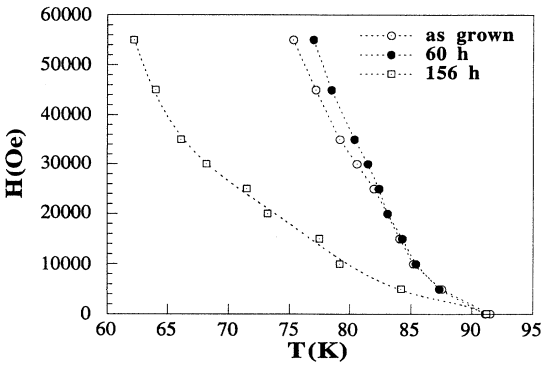

FIG. 9. Shift of the irreversibility line as a function of the O_2 annealing time in the $\mathbf{H}\|c$ configuration.

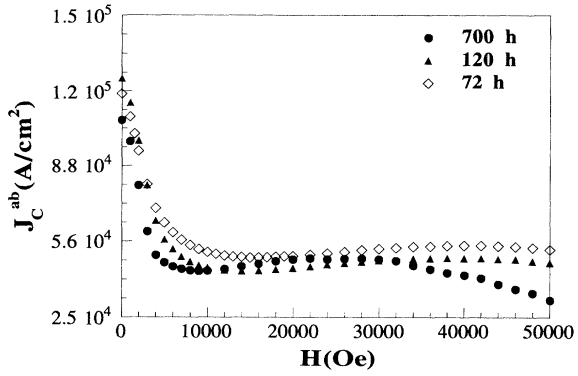

FIG. 10. Field dependence of the critical currents as a function of the annealing time in the $\mathbf{H}\|c$ configuration for the sample with 14% of 211 phase ($T=60$ K).

rate of the critical currents seems to be smaller in this case, thus pointing to the fact that the observed microstructure evolution is enhanced when increasing the concentration of 211 precipitates. Furthermore, the anomalous fishtail effect of the field dependence of the critical currents becomes more apparent with the aging process. This is also an indication of the fact that a precise knowledge of the microstructure is necessary to analyze these magnetization anomalies.

IV. DISCUSSION AND CONCLUSIONS

A. Aging of the microstructure during the oxygenation process

Our results presented above indicate that the 123 matrix undergoes severe plastic deformation when the composite is submitted to an annealing process at 450 °C in an O_2 flow for several days. The process is accompanied by extensive dissociation of dislocations, which in turn is associated with the nucleation of extrinsic stacking faults at the dislocation cores. Such extrinsic defects then become a dominant microstructural feature.

The contrast behavior of the partial dislocations bounding the stacking faults indicates an exchange of the in-plane shear component of the **R** vector between the *a* and *b* axes across the twin boundaries. It should be noted that the aging process is performed within the stability range of the bulk 124 phase, that is, below 840 °C,[18] and therefore there is a thermodynamic driving force for the formation of 124 faults. It has been argued, however, that strain considerations are likely to inhibit the segregation of the 124 phase into separated domains.[19] In the 124 structure, the shear between the two consecutive CuO chain layers is along the *b*-axis direction. Therefore, if as expected for the present case the stacking faults were formed in the orthorhombic phase, the lower-energy stacking-fault configuration would yield a $\sim 90°$ rotation of the shear component across the twin boundaries, which is not observed in our experiments. In fact, an exchange of the shear components across the twin boundaries would be expected for a stacking fault formed in the tetragonal phase provided that the *a* and *b* axes are then crystallographically equivalent. Our observations thus suggest an accommodation of the shear exchange by the formation of $\frac{1}{2}\langle 110\rangle$ screw dislocations parallel to the twin boundaries, satisfying the dislocation reaction[10,20]

$$\tfrac{1}{6}[031]+\tfrac{1}{2}[1\bar{1}0]\rightarrow\tfrac{1}{6}[301]$$

This mechanism is then considered to cost less energy than an in-plane rotation of $\sim 90°$ of the **R** vector at every twin boundary under the conditions in which the annealing process takes place.

The final size of the stacking faults (and therefore their growth rate) is diffusion limited and we have observed that it strongly depends on the type of defect from which they were originated. On the other hand, since the nucleation of a stacking fault in the perfect matrix always costs more energy than its nucleation in a dislocation core, the generation of stacking faults within the bulk perfect 123 matrix is not a relevant process even after prolonged aging periods, as demonstrated by the small size of the loops shown in the inset of Fig. 3(a). In particular, our results indicate that the size of the stacking faults increases when they are associated with low-angle grain boundaries and 211/123 interfaces, as compared with the corresponding sizes found in dissociated dislocation segments located within the bulk 123 matrix (typically less than 80 nm), where pipe diffusion along the dislocation core is probably the unique feeding mechanism for the growth of the extra CuO chain layer. Therefore the development of the aged microstructure has to be addressed from consideration of the topological distribution of such defects in the parent nonaged microstructure.

Our directionally solidified bars are characterized by dense and homogeneous distribution of fine 211 precipitates,[21] which is accompanied by a uniform polygonization process resulting from the thermal contraction of the sample.[5] Low-angle grain boundaries have been shown to be a dislocation source in both such 123/211 composites[5] and 123 single crystals.[14] It was observed that small stacking faults associated with the low-angle grain boundaries widened noticeably after keeping single-crystal TEM samples for six months in air,[14] indicating that atomic mobility along low-angle grain boundaries may be effective even in ambient conditions. The high density of low-angle grain boundaries present in our samples thus may be considered to play a major role in the development of defect structures associated with the aging process.

Our samples are also characterized by a high effective 211/123 interface area as well as a high density of small microcracks which typically stop at the 211/123 interfaces, and both defects constitute the preferential diffusion path for oxygen. Thus the presence of the large stacking faults observed along the [001] zone axis in Fig. 3(a) can be understood in terms of an enhanced atomic diffusion along 211/123 interfaces, in particular associated with the presence of neighboring microcracks [either above or below the view plane of Fig. 3(a)]. In a similar

way, we can speculate that the degraded region arrowed in Fig. 3(a) corresponds to the degradation zone associated with a neighboring precipitate which was located either above or below the view plane.

The formation of stacking faults implies a local CuO enrichment within the 123 matrix, and therefore in order to preserve the overall composition of the matrix the concentration of copper in some regions of the matrix should drop. However, there is yet no experimental evidence for the existence of such copper-depleted regions. Taking into account the observed preferential location of the stacking faults, the most likely source of copper atoms for their growth are the degraded regions observed at either side of the microcracks and the degradation products present within their gaps and at their intercepts with the 211 precipitates.

Our TEM observations support the idea that the aging process is enhanced when the density of small 211 precipitates is high because then the total 211/123 interface area and the density of small-angle grain boundaries as well as the density of small microcracks are increased, and all these defects constitute places where the degradation of the matrix is accelerated.

Finally, an important conclusion to be drawn concerning the mechanical performance of these materials is that for oxygenation periods exceeding the optimum ones, the 211 precipitates cease to be operative in stopping the microcracks, thereby decreasing the mechanical toughness of the composite. Implications for the superconducting properties of such a degraded microstructure are addressed below.

B. Implications for the superconducting properties

It is evident from Figs. 6–10 that a large change of the irreversible superconducting features has occurred as a consequence of the annealing process in O_2. The origin of this strong deterioration of the superconducting performance lies in the severe modification of the microstructure that takes place in the oxygenation step, as we have discussed above. One important point to bear in mind when analyzing the properties of the samples is that, as a result of the intrinsic anisotropy of the oxygen diffusion constants, oxygenation occurs much faster along the (001) planes; additionally, the existence of microcracks further increases the oxygen diffusion parallel to these planes. In the case of oxygen-deficient samples these circumstances add up to generate layeredlike structures in which fully and partially oxygenated areas may coexist.[2]

On the other hand, as we have discussed above, an excessive oxygenation of the melt-textured 123 samples leads to the formation of degraded regions associated with the microcracks as well as stacking faults and dislocations. Since microcracks are parallel to the *ab* planes the aging process generates a superconducting layeredlike structure in which strongly degraded bands parallel to the *ab* planes, having a substantial cross section perpendicular to the *c* axis, occur. The existence of this layeredlike structure is confirmed by the low-field susceptibility measurements in the aged sample containing 36% 211, which show a strong reduction of the magnetic shielding capability in the $\mathbf{H}\|ab$ configuration (see Fig. 6). The fact that the shielding is complete in all the other samples when $\mathbf{H}\|ab$ gives further support to our previous assessment that the degradation rate is enhanced in samples having a higher concentration of 211 particles. When the concentration of 211 particles is augmented the separation between microcracks along the *c* axis is smaller, even if these microcracks are shorter and thinner. Then, in this case the layered degraded zones will have a higher density in the 123 matrix and they will come into contact more often, as shown above, thus avoiding the shielding currents to flow along the *c* axis.

Once the layeredlike structure of the samples has been established we can analyze the remaining observed features of the superconducting properties. Regarding the critical currents in the low-field region, the law expected for surface core pinning, $J_c = AH^{-1/2}$,[22] still gives a proper description of the field dependence of the critical current (see Fig. 11). A linear term of the form $(1-H/H_{\rm irr})$ has also been used to take into account the presence of the irreversibility line. The fact that in this field region the critical currents show a small dependence on the annealing time indicates that 211/123 interface pinning, the dominant pinning mechanism in this region,[23,24] is not severely affected. Actually, in the $\mathbf{H}\|c$ configuration the *A* coefficient slightly decreases (about 25%) with increase of the annealing time, while the contrary occurs for the $\mathbf{H}\|ab$ configuration. These observations may shed some light on the controversy concerning the pinning mechanism associated with the 211 particles in melt-textured 123 (i.e., the 211/123 interface or the associated defects). The fact that the *A* parameter decreases when a higher concentration of planar defects exists in the 123/211 interface is a clear indication that the dominant mechanism is the interface itself. Since both matrix degradation and stacking faults propagate layerwise along the *ab* planes, their presence associated with the 211/123 interfaces is likely to result in a decrease of the superconducting order parameter across such interfaces preferentially in the directions contained in the *ab*

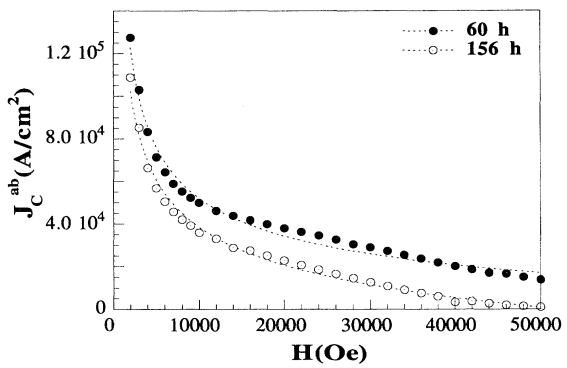

FIG. 11. Field dependence of the critical current at $T=60$ K in the $\mathbf{H}\|c$ configuration. The lines correspond to the fit $J_c \approx AH^{-1/2}(1-H/H_{\rm irr})$.

planes, thus decreasing the individual pinning force when the fluxoids are directed along the c axis, i.e., in the $\mathbf{H}\|c$ configuration.

In the high-magnetic-field region the 123/211 interfaces can no longer pin all the vortices and the defects existing in the matrix regions separating 211 particles, namely, dislocations, stacking faults, and nonsuperconducting bands, are then expected to contribute to the field dependence of the critical currents. It has been shown by Selvamanickam, Mironova, and Salama[7] that dislocations enhance the critical currents in this field region. However, the observation of a decrease of $J_c^{ab}(H)$ in the high-field region in the aged samples [see Fig. 8(a)], indicates that the degradation of the superconducting matrix dominates the overall behavior of $J_c^{ab}(H)$, even if the concentration of dislocations is as high as that observed in the mechanically deformed samples.[7] This may be understood if we take into account that the nonsuperconducting areas gradually increase the two-dimensional behavior of the vortex lattice in the $\mathbf{H}\|c$ configuration. Then thermal activation effects become further increased and the situation mimics that observed in artificial superlattices[25] in which thermal effects become strongly enhanced when the thickness of the nonsuperconducting layers increases. This enhancement of the two-dimensional behavior is reflected in a stronger field dependence of the critical current and in a dramatic downward shift of the irreversibility line, as we have observed in our aged sample.

On the other hand, when looking at the field dependence of the critical current $J_c^c(H)$, i.e., when $\mathbf{H}\|ab$, the observed behavior may be explained by considering the progressive formation of a decoupled layered structure in which the area where the critical state takes place becomes smaller. The decoupling of currents flowing along the c-axis direction occurs progressively as the field increases. At low fields the shielding currents flowing along the c-axis direction percolate but the overall shielded volume is small because the currents have a meander-like path. In this field region the critical state is established across all the sample. Thus, if the pinning mechanism remains essentially the same, the critical currents must be essentially unchanged by the aging process, as was indeed observed. Only a small increase of the A coefficient in the law $J_c^c = AH^{-1/2}$ has been observed, which, if we take into account that the Lorentz force is parallel to the ab planes, can be explained by considering the pinning of the vortices by the dislocation lines lying on the ab planes and the $\frac{1}{6}[301]$ partial dislocations bounding the stacking faults introduced in the aging process.[7] When the magnetic field is increased, the induced currents will reach the critical current much more easily in the narrow regions separating the nonsuperconducting degraded zones and then the critical state settles in a smaller volume, thus leading to a reduction of the calculated inductive critical currents $J_c^c(H)$. A similar observation has been reported by Kresse *et al.* by means of flux profile measurements of melt-textured 123 at high fields and temperatures.[26] The same explanation may also account for the observed downwards shift of the irreversibility line in this configuration.

It is worth mentioning that the effects associated with the progressive increase of superconducting degraded zones with annealing time are also evident in the sample with low 211 phase content ($\approx 14\%$). This sample exhibits the anomalous fishtail effect when $\mathbf{H}\|c$, first related to the existence of local fluctuations of the oxygen content.[1] The fishtail effect becomes apparent and more pronounced as the annealing time increases, thus clearly indicating that a relation exists between this anomalous $J_c^{ab}(H)$ dependence and the microstructural features of the samples. It is very unlikely, however, that poorly oxygenated regions persist in the samples after long oxygenation periods and it seems more likely that the new dislocations created during the annealing process could be active pinning centers at high magnetic fields,[7,8] thus retarding the overall decrease of $J_c^{ab}(H)$ which we have associated with an enhanced two-dimensional behavior.

In summary, we have shown that the oxygenation process in melt-textured 123/211 composites may have a strong influence on the irreversible superconducting properties because there is an important aging of the microstructure. The most prominent effect is the creation of large stacking faults and dislocations together with an intense degradation of the matrix associated with the microcracks and the 211/123 interfaces. We also show that the relevance of the aging process strongly depends on the content of 211 phase and the concomitant modification of the parent microstructure of the ceramic composite, but, in any case, the effects are mostly visible at high magnetic fields. From a practical point of view, this work demonstrates that different oxygenation processes will be necessary to optimize the critical currents in samples having modified microstructures.

ACKNOWLEDGMENTS

This work has been supported by the MIDAS program (93-2331), CICYT (MAT91-0742), and EC-BE-8068. We are very grateful to Dr. J. Portillo and Dr. Y. Mariette (Serveis Científico Tècnics de la Universitat de Barcelona) for assistance during TEM experiments, and to Dr. J. Fontcuberta and Dr. F. de la Cruz for interesting discussions.

[1] M. Daeumling, J. Seuntjens, and D. C. Larbalestier, Nature **346**, 16 (1990).

[2] B. Martínez, V. Gomis, S. Piñol, I. Catalán, J. Fontcuberta, and X. Obradors, Appl. Phys. Lett. **63**, 3081 (1993).

[3] Y. Zhu, R. L. Sabatini, Y. L. Wang, and M. Suenaga, J. Appl. Phys. **73**, 3407 (1993).

[4] S. Piñol, V. Gomis, A. Gou, B. Martínez, J. Fontcuberta, and X. Obradors, Physica C (to be published); B. Martínez, F. Sandiumenge, S. Piñol, N. Vilalta, J. Fontcuberta, and X. Obradors, Appl. Phys. Lett. (to be published).

[5] F. Sandiumenge, S. Piñol, X. Obradors, E. Snoeck, and Ch. Roucau, Phys. Rev. B **50**, 7032 (1994).

[6]M. J. Kramer, R. W. McCallum, W. J. Nellis, and U. Balachandran, Physica C **228**, 265 (1994).
[7]V. Selvamanickam, M. Mironova, and K. Salama, J. Mater. Res. **8**, 249 (1993).
[8]M. Ullrich, D. Muller, W. Mexner, M. Steins, K. Heinemann, and H. C. Freyhardt, Phys. Rev. B **48**, 7513 (1993).
[9]J. Rabier, P. D. Tall, and M. F. Denanot, Philos. Mag. A **67**, 1021 (1993).
[10]J. Rabier and M. F. Denanot, Philos. Mag. A **65**, 427 (1992).
[11]B. Domenges, M. Hervieu, C. Michel, and B. Raveau, Europhys. Lett. **4**, 211 (1987).
[12]J. Tafto, M. Suenaga, and R. L. Sabatini, Appl. Phys. Lett. **52**, 667 (1988).
[13]Z. L. Wang, A. Goyal, and D. M. Kroeger, Phys. Rev. B **47**, 5373 (1993).
[14]H. Gu, C. Colliex, S. Senoussi, C. Aguillon-Levillain, and P. Manuel, Philos. Mag. A **68**, 19 (1993).
[15]R. K. Williams, K. B. Alexander, J. Brynestad, T. J. Henson, D. M. Kroeger, T. B. Lindemer, G. C. Marsh, J. O. Scarbrough, and E. D. Specht, J. Appl. Phys. **70**, 906 (1991).
[16]N. Chen, S. J. Rothman, J. L. Routbort, and K. C. Goretta, J. Mater. Res. **7**, 2308 (1992).
[17]S. Piñol, J. Fontcuberta, B. Martínez, and X. Obradors, in *Applied Superconductivity,* edited by H. C. Freyhardt (DGM-I Verlag, Oberursel, 1993), p. 377.
[18]J. Karpinski, E. Kaldis, E. Jilek, S. Rusiecki, and B. Bucher, Nature **336**, 660 (1988).
[19]A. F. Marshall, K. Char, R. W. Barton, A. Kapitulnik, and S. S. Laderman, J. Mater. Res. **5**, 2049 (1990).
[20]J. Rignalda, C. J. Kily, P. Fox, and G. J. Tatlock, Philos. Mag. A **69**, 729 (1994).
[21]S. Piñol, F. Sandiumenge, B. Martínez, J. Fontcuberta, and X. Obradors, Appl. Phys. Lett. **65**, 1448 (1994).
[22]A. M. Campbell and J. E. Evetts, Adv. Phys. **21**, 199 (1972).
[23]M. Murakami, K. Yamaguchi, H. Fujimito, N. Nakamura, T. Taguchi, N. Koshizuca, and S. Tanaka, Cryogenics **32**, 930 (1992).
[24]V. Gomis, S. Piñol, B. Martínez, J. Fontcuberta, and X. Obradors, in *Applied Superconductivity* (Ref. 17), p. 373; B. Martínez *et al.* (unpublished).
[25]O. Brunner, L. Antognanza, J. M. Triscone, L. Mieville, and O. Fischer, Phys. Rev. Lett. **67**, 1354 (1994).
[26]R. Kresse, H. Kupfer, R. Meier-Hirmer, T. Matsushita, and K. Kimura, in *Applied Superconductivity* (Ref. 17), p. 337.

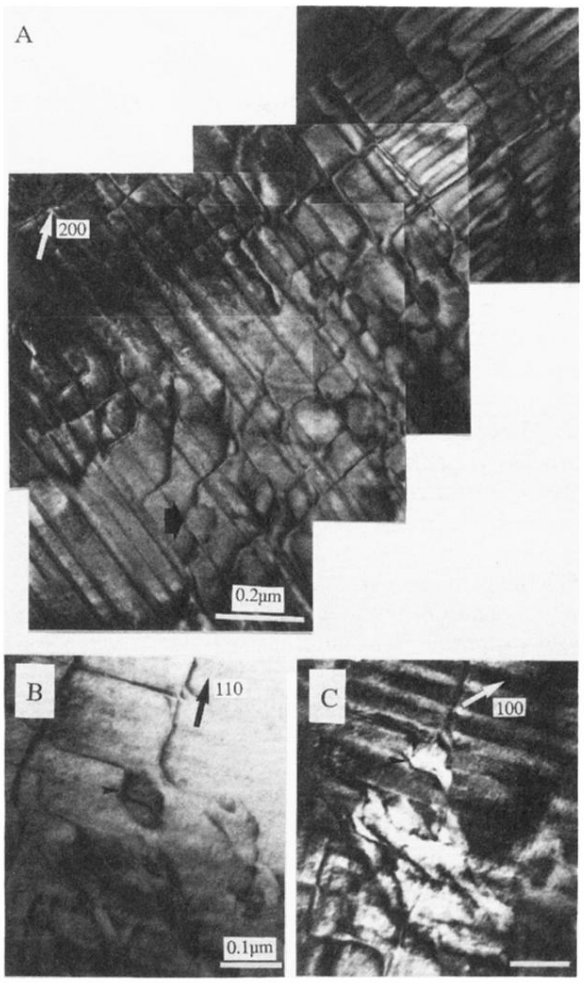

FIG. 1. (a) Bright-field image obtained with the 200 reflection near the Bragg position showing extensive dislocation dissociation; (b) bright field, $\mathbf{g}=110$; (c) bright field, $\mathbf{g}=100$.

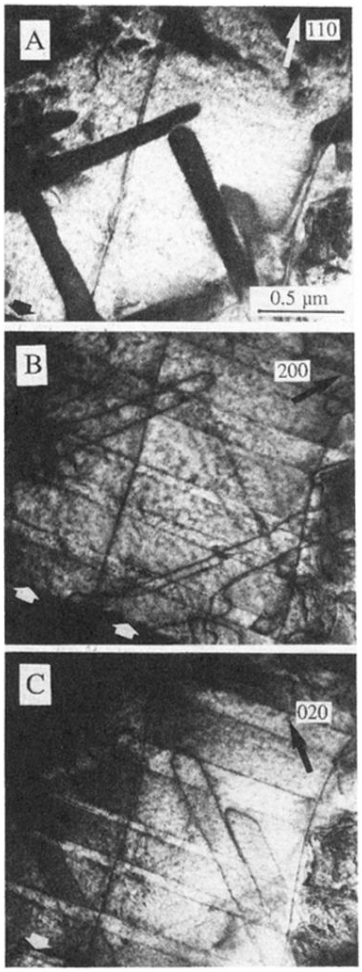

FIG. 2. Two-beam bright-field images of stacking faults originating from a low-angle grain boundary imaged with the 110 (a), 200 (b), and 020 (c) reflections at the Bragg position.

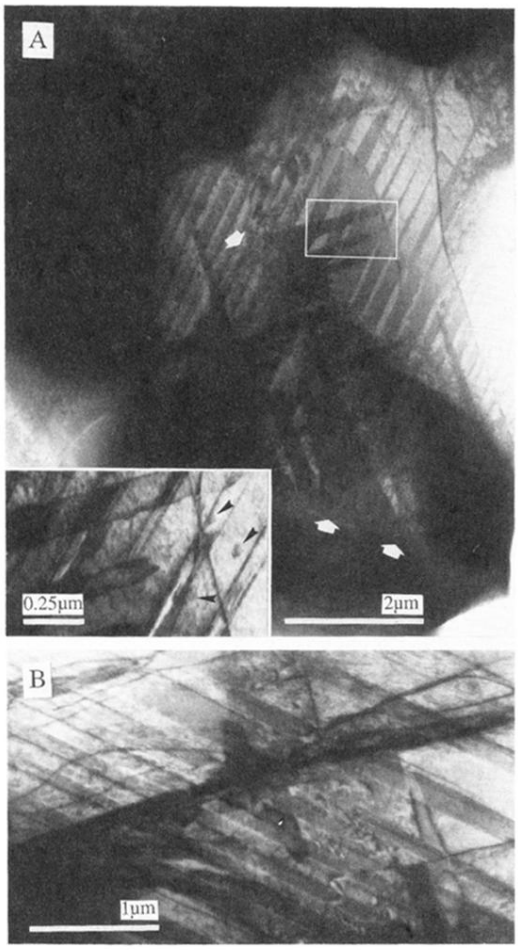

FIG. 3. (a) Large stacking faults elongated in the [100] and [010] directions originating from 211/123 interfaces and a degraded zone (arrowed). The inset is an enlarged view of the region enclosed by white borders, where small dislocation loops are indicated by arrow heads. (b) Similar stacking faults originating from a dislocation tangle.

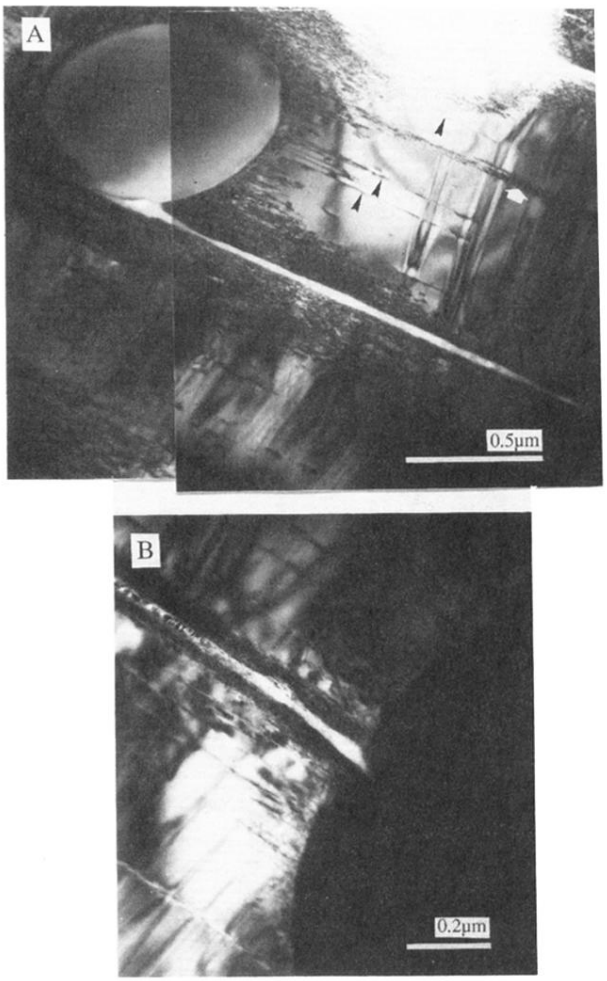

FIG. 4. Interaction of a microcrack with a 211 precipitate with associated thick degraded layers viewed along the [100] direction: (a) aged sample, oxygenated for 156 h, and (b) nonaged sample, oxygenated for 60 h.

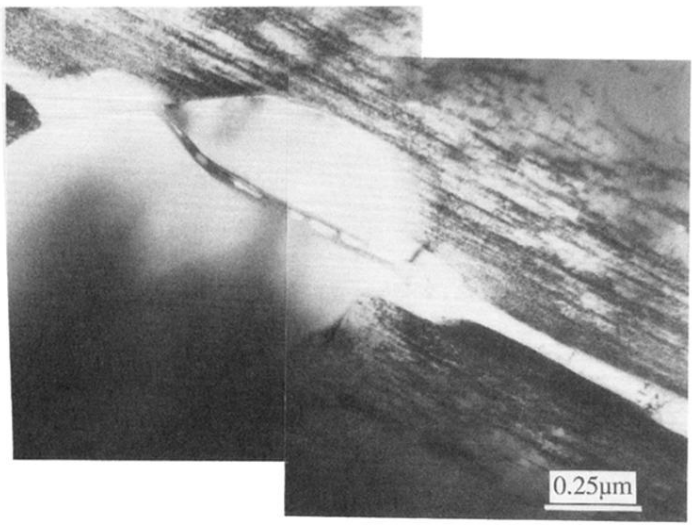

FIG. 5. Microcrack propagating across a 211 particle.